## Fabrication of a Ti-based 3D porous transport layer for PEMWEs using ShockWave-induced spraying and cold spray

Fakourihassanabadi, Mohsen; Guerreiro, Bruno; Gaudet, Julie; Martin, Manuel H.; Abbasi, Somayyeh; Thorpe, Steven; Guay, Daniel



**Publisher's version / Version de l'éditeur:**
https://doi.org/10.1016/j.surfcoat.2023.130353
*Surface and Coatings Technology, 477, C, pp. 1-9, 2023-12-29*

# Fabrication of a Ti-based 3D Porous Transport Layer for PEMWEs Using ShockWave-Induced Spraying and Cold Spray

Mohsen Fakourihassanabadi[1], Bruno Guerreiro[2], Julie Gaudet[1], Manuel H. Martin[2], Somayyeh Abbasi[1], Steven Thorpe[3], Daniel Guay[1*]

[1] Institut national de la recherche scientifique, Énergie, matériaux et télécommunications 1650 Lionel Boulet Blvd. Varennes, QC Canada J3X 1P7

[2] National Research Council of Canada, 75 de Mortagne Blvd., Boucherville, QC, Canada J4B 6Y4

[3] Department of Materials Science and Engineering, University of Toronto, 184 College Street, Toronto, ON M5S 3E4 Canada.

Cost-effective production of green hydrogen is contingent upon reducing the capital cost of Polymer Electrolyte Membrane Water Electrolysers (PEMWE). Currently, 17 to 25% of the production cost of a PEMWE stack depends on components related to the Porous Transport Layer (PTL). PTLs are usually made of compressed and sintered titanium powders/fibers to provide them with structural and chemical integrity with carefully controlled interconnected porosity. Herein, we report on the preparation of Ti-based PTLs produced by Shock-Wave Induced Spray (SWIS) and Cold Gas Dynamic Spray (CGDS), two deposition processes that does not require any subsequent heat treatment. This report investigates the effect of using porogens to control the porosity of the Ti-based PTLs. Two porogens, Cu and Al, were used to investigate the effect of porogen density on the deposition efficiency and porosity of the resulting coatings. The Al porogen allowed for the production of Ti-based PTLs coatings with *ca.* 60% porosity, which is a very desirable feature for producing PTLs with high gas permeability.

* Corresponding author: daniel.guay@inrs.ca

## 1. Introduction

Green hydrogen production through water electrolysis, when linked with renewables such as wind and hydro, displays low environmental impact and is essential to reach global decarbonization goals by 2050 [1, 2]. With the falling cost of renewable energy sources, the capital cost of the electrolyser itself is of prime concern. Proton Exchange Membrane Water Electrolysers (PEMWE) are widely regarded as the leading technology for water splitting. Due to the acidic environment in PEMWE, platinum group metal (PGM) electrocatalysts and corrosion-resistant materials are required as components in the anodic side of the cell [3].

The energy efficiency of PEMWEs is reflected by the cell overpotential that is derived from three major contributions: the activation overpotentials that correspond to the anodic and cathodic electrochemical reactions; the ohmic overpotential related to the resistance in the system (electrolyte, connections, etc.); and the mass transport overpotential related to the transport of reactants (water) and reaction products (hydrogen and oxygen) [4]. Here, we focus on the porous transport layer (PTL), which is responsible for transporting water molecules and the gaseous reaction products (hydrogen and oxygen) to and from the electrocatalyst surface, respectively. The anode PTL represents approximately 9-15% of the production cost of a PEMWE stack [5] and contributes to *ca.* 30% of the mass transport overpotential [6].

For proton exchange membrane water electrolysis, PTLs should have several characteristics, including high electrical and thermal conductivity to reduce the ohmic resistance and prevent membrane thermal damage. Also, as current density increases, oxygen bubbles can accumulate in the PTL pores, hindering the transport of water molecules to the active sites of the

anodic electrocatalyst. It is therefore important that the PTL facilitates the removal of oxygen bubbles so as not to impede the transport of water molecules to the electrocatalyst surface. [7].

Important design criteria for the fabrication of PTLs include the type of material, porosity, pore size, and pore connectivity [8, 9, 10, 11, 12, 13]:

i. While carbon materials can be used for cathode PTLs, state-of-the-art materials for anode PTL are titanium-based due to the high anodic potential reached. Titanium has very high corrosion resistance in the acidic environment of the PEMWE, good electrical and thermal conductivity, and high specific strength [14, 15, 16].
ii. Porosity is important for allowing the reactants and the products to reach and leave the electrocatalytic sites. A balance should be found in the two phase field flow (water molecules in and oxygen gas out). An excessively small porosity will hamper the flow of both reactants and products, while an excessive large porosity can lead to oxygen gas saturation of the PTL and difficult access of water molecules to the electrocatalytic sites, thereby reducing the PEMWE performance [17, 18]. In the literature, the optimum porosity lies between 50 and 75% [19].
iii. Pore size and ohmic resistance are linked. An increase in pore size leads to an increase in ohmic resistance and thus to a decrease in PEMWE performance. Higher ohmic resistance can also lead to greater energy loss in the form of heat, which can create hot spots and local membrane degradation. [9]. Mo *et al.* also reported that OER occurred only at the point of contact between the PTL and the catalyst-coated membrane, highlighting the importance of reducing the pore size and the distance separating them in order to maximize the contact area between the PTL and the catalyst-coated membrane [20]. However, pores that are too small can reduce

PEMWE performance by delaying/preventing the rapid removal of gas bubbles. For PTLs produced by the powder metallurgy process, an optimal pore size of 10 μm was reported [10].

iv. Pore connectivity is also critical for the performance of PEMWEs to increase the permeability of water molecules and oxygen gas (two-phase flow) [7].

PTLs can be fabricated by different processing methodologies, including furnace-sintering metal powders, lithography, tape casting, and vacuum plasma spraying [10, 17, 21]. Although lithography allows the creation of well-defined 3D structures, the process is time-consuming and labor-intensive. Furnace-sintering metal powders and tape-casting technologies require considerable manufacturing time and incurred costs [23]. Vacuum plasma spraying (VPS) has also been studied as it offers the advantage of removing the heat treatment step. In VPS, the powders are melted and accelerated by a plasma jet and directly impact the substrate surface producing a porous structure with good metallurgical bonding. Also, VPS deposition conditions can be determined to minimize the oxidation of the melted powders [24]. However, in the literature, the porosity of PTL prepared by VPS is limited to less than 30% [25].

This study investigated the production of PTL by cold gas dynamic spray coating (CGDS) [26] and Shock-Wave Induced Spraying (SWIS) process [25] which offer the advantages of VPS without powder melting. In CGDS, the particles are accelerated in a supersonic gas to achieve high velocity before impacting the surface. The particle temperature remains below the melting point lowering the risk of microstructural change and oxidation of the compound [26, 27, 28]. The particles are considerably deformed due to the high velocity which limits the porosity in the coating to less than 30% [26, 27, 28].

Shock-Wave Induced Spraying (SWIS) process is another method for producing porous coatings. This process combines the benefits from both VPS and CGDS. In the SWIS process, the rapid opening and closing of a valve generates a series of shock waves. The shock waves travel through the spray gun accelerating and heating the powder within the gun. The particles then impact the substrate like in CGDS but at a higher temperature than CGDS [29]. Consequently, higher bonding strength can be achieved at lower powder speeds than in CGDS resulting in larger porosity [25].

In the preparation of porous substrates, a porogen acts as a sacrificial template that increases the porosity of the coating when removed by heat treatment or leaching processes. J. Sun *et al.* prepare a porous cold spray coating with a porosity of 49% by cold spraying a Ti + Mg mixture, then heat treating it in a vacuum chamber at 1250°C to evaporate the Mg [30]. Qiu *et al.* also prepared a porous cold spray coating with 48% porosity by cold spraying a mixture of Ti + Al and then removing Al in a NaOH solution [31]. The advantage of the leaching process over sintering is that it can be carried out at room temperature, which reduces the risk of oxidation and microstructure modification.

In the present work, CGDS and SWIS processes were used to prepare Ti porous coatings. Aluminum and copper particles were used as porogen materials. Both porogens were removed using a leaching process.

## 2. Experiment

### 2.1. Material

Three different Ti powders with different particle sizes and two types of porogen, namely Cu and Al powders, were used throughout the present study. The characteristic of the powders

used for deposition are presented in Table 1. The deposition of Ti coating was carried out on mild steel substrates (76.2 mm x 76.2 mm x 6.5 mm). Prior to deposition, the substrates were cleaned with ethanol and grit blasted with alumina.

Table 1: Characteristic of the powders used for the deposition.

| Material | Producer | Purity | Particle Size (D50) |
|---|---|---|---|
| Ti | AP&C | > 99.5% | 30 μm |
| Ti | Wah Chang | ------ | 73 μm |
| Ti | Goodfellow | > 99.5% | 90 μm |
| Al | Equispheres | > 91%, 7 wt.% Si | 83 μm |
| Cu | Metco | > 99.3% | 70 μm |

**2.2. Deposition techniques**

The Shock-Wave Induced Spray (SWIS) deposition system was supplied by Centerline Ltd. It used a stainless-steel tube nozzle (650 mm long with 5 mm internal diameter) connected to a divergent stainless-steel tube coated with Inconel (5 mm inlet diameter, 6 mm outlet diameter, and 120 mm long). The Cold Gas Deposition System (CGDS) system was from Kinetiks 4000 from CGT-GmbH, currently part of Impact-Innovations, Germany. It used a SiC nozzle. Nitrogen gas was used as the carrier gas in both of these processes.

### 2.3. Deposition of Ti powder using the SWIS technique

In a first set of experiments, three Ti powders of different sizes were deposited on the surface of mild steel substrates using the SWIS process to find the optimal size to maximize the porosity of the resulting coating. Table 2 provides the deposition parameters used for this first set of experiments.

Table 2: Deposition parameters

| Powder | Ti | Ti + Cu | | Ti + Al |
|---|---|---|---|---|
| Spray System | SWIS | SWIS | CGDS | SWIS |
| Gas Nature | $N_2$ | $N_2$ | $N_2$ | $N_2$ |
| Gas Temperature (°C) | 600 | 600 | 650 | 550-600 |
| Gas Pressure (psi) | 600 | 600 | 580 | 550-600 |
| Valve Frequency (Hz) | 25-30 | 30 | --- | 30 |
| Stand-Off Distance (mm) | 25 | 25 | 25 | 25 |
| Powder Pre-Heating (°C) | 600 | 600 | None | None |
| Powder Feeder Wheel Speed (rpm) | 0.25-1 | 1 | 1 | 0.5-3 |
| Traverse Speed (mm/s) | 10-100 | 100 | 300 | 10-100 |
| Step Size (mm) | 1 | 1 | 1 | 1 |

### 2.4. Deposition of Ti + Cu mixture powder and leaching process

In a second series of experiments, Ti powder with 73 μm diameter was blended with 5, 30 and 60 wt.% Cu. This powder mixture was deposited on the surface of mild steel substrates. A first series of deposits were prepared using the SWIS process, while a second series of deposits were prepared using the CGDS process. The deposition parameters are given in Table 2. In some cases, these samples were immersed in 5M $HNO_3$ for one hour under stirring conditions, resulting in the formation of self-standing coatings. The latter were then washed in boiling de-ionized water for one hour under stirring conditions.

### 2.5. Deposition of Ti+ Al mixture powder and leaching process

In a third series of experiments, Ti powder with 73 μm diameter was blended with 20, 30 and 40 wt.% Al. This powder mixture was deposited on the surface of mild steel substrates using the SWIS process with the parameters given in Table 2. To remove Al from the coating, the samples were immersed in a freshly prepared 6M NaOH solution held at 70-90℃ for one hour. Following that, the samples were rinsed for 1 h in boiling de-ionized water. This step was repeated three times. Then, the samples were immersed for an hour in 0.5 M $H_2SO_4$ under stirring to detach the substrate from the coating and rinsed 1 h in boiling de-ionized water. This procedure was repeated until the coating was detached from the substrate. Finally, step one was repeated two times to make sure Al was completely dissolved.

### 2.6. Physical characterization

The coatings were mounted in resin, then sectioned and polished. Optical microscopy images were taken using an Olympus microscope equipped with automatic image capture software. To assess porosity, optical microscopy images of the entire coating were acquired using

the software's Automated Stitched mode, at 50X magnification (Figure S1). Next, a threshold technique was employed to identify pores in the sample. Porosity was then determined by dividing the surface area of identified pores by the total surface area.

Scanning Electron Microscopy (SEM, JEOL, JSM-6300F) and Energy Dispersive X-Ray (EDX, VEGA3 TESCAN) measurements were carried out before and after leaching to visualize and quantify the different elements. All SEM images were taken in secondary electron mode. EDX analysis was conducted on the coatings at a magnification of 55X and at three distinct spots on each sample. The resulting data were then used to calculate the average content of Al or Cu in the coatings.

## 3. Results

### 3.1 Particle size and morphology

Fig.1 shows the particle size distribution of all powders used in the present study. The D50 value of the Ti powders were 30, 73 and 90 μm, while that of Cu and Al were 70 and 83 μm. Fig.2 depicts the SEM micrographs of the same powders. The Al, Cu and Ti with D50 = 30 μm were spherical in shape with a smooth surface texture. By contrast, the Ti powder with D50 = 70 μm and 90 μm both have an irregular shape with several sharp edges and faceted surface texture.

### 3.2 Porosity of pure Ti powder samples by the SWIS technique

The Ti powders were sprayed onto mild steel substrates to determine the effect of particle size on the porosity of the resulting coating. Fig.3 showed cross-sectional SEM micrographs of the resulting coating prepared by the SWIS process. The grey areas are the Ti powders while the black areas are the epoxy filled pores. The porosity of the different coatings are summarized in Table 3.

Table 3: Porosity of the SWIS coatings prepared using different Ti particle sizes

| Powder | Porosity (%) |
|---|---|
| Ti 30μm | 25 ± 3 |
| Ti 73μm | 38 ± 4 |
| Ti 90μm | 39 ± 4 |

The porosity of the coatings increased with increasing Ti particle size from 30 to 73 μm. However, this effect levels off as the Ti particle size is further increased. In the SWIS process, it is expected that the impact velocity of the particles decreases with increasing particle size [32, 33, 34, 35], which leads to a reduction of the particle deformation at the point of impact and an increase of the coating porosity [36, 37]. Under our operating conditions, the maximum coating porosity that can be achieved by changing the Ti particle size is 40%. When a drop of water is deposited on the surface of the coatings, the water passes through the coating, showing that the pores are interconnected.

### 3.3 Effect of Cu porogen on the porosity of Ti coatings prepared by the SWIS technique

In an effort to further increase the porosity of the Ti-based cotaing, Cu was used as a porogen. Figure 4 depicts the cross-sectional SEM micrographs of the Ti + Cu coatings produced by the SWIS technique. The gray particles are Ti and the white particles are Cu. The Cu particles are dispersed homogeneously in the as-deposited coating. After leaching in $HNO_3$, most of the Cu particles were dissolved and only a few white (Cu) particles were observed in the coating with the largest Cu content (Figure 4f).

The relationship between the Cu content in the powder mixture with that of the as-deposited coatings was assessed by EDX measurements. As seen in Figure 5a, an increase in the Cu content in the powder feeder caused an increase in the Cu content of the coating, although there is not a one-to-one relationship between both parameters. Previous reports have shown that the composition of a coating made of two different materials A and B depends on the A and B content in the powder feeder and the ratio of the Deposition Efficiency (*DE*) of A and B, $\frac{DE_A}{DE_B}$. The deposition efficiency depends on the particle impact velocity and critical velocity. This critical velocity represents the minimum required particle velocity for material deposition onto a surface. [33]. Furthermore, in the case of mixed powders, when the mechanical and physical properties of two powders are significantly different, the interaction between the two different powders can affect the chemical composition of the coating [38].

To determine the *DE* of Cu, Cu particles with D50 = 70 μm were deposited on mild steel using the SWIS parameters detailed in Table 2. No Cu deposit could be formed. In our experimental conditions, the *DE* of Cu is negligible, most probably because the Cu particles could not reach a velocity exceeding the critical velocity. Indeed, in the same experimental conditions, it was only possible to obtain a Cu deposit when Cu particles with D50 = 50 μm were used, consistent with the fact that particles with smaller D50 will have lower mass and thus increase velocity compared to particles with larger D50. In our experimental conditions, Cu particles with D 50 = 70 μm were most probably entrapped within the Ti coating, explaining the low Cu content in the as-deposited coating.

As shown in Figure 5b, an increase of the Cu content in the powder feeder decreased the porosity of the resulting coating. The decrease of the coating porosity with the Cu content of the

feeder is most probably due to Cu particles occupying the pores between the Ti particles. This would be consistent with the fact that, in our deposition conditions, the Cu particles are not accelerated enough to be deformed upon impacting the substrate.

After leaching, all coatings separated from the substrate because the corrosion rate of mild steel in $HNO_3$ is large [39]. As noted above, there are almost no Cu particles left in the coating after leaching, indicating that the acidic solution had access to both the surface and the bulk of the coating. Permeation of the acidic solution to the bulk of the coating was favored by the initial porosity of the coating, which resulted from the use of Ti particles with D50 = 73 μm. Even the thickest coatings investigated were not damaged nor cracked after the leaching process (Figure S2). This is consistent with the fact that Cu particles are only trapped in Ti coatings and do not contribute to the mechanical properties of the coating. Consequently, their dissolution during acid treatment has no effect on the coating's mechanical properties. As expected, leaching of Cu particles from a coating increased its porosity (Figure 5b). However, this increase is such that the porosity of the film after leaching does not exceed *ca.* 40%, which is equivalent to the porosity of coatings prepared using only Ti particles of the same size.

Clearly, with the SWIS deposition technique, there is no benefit of using a Cu porogen to prepare porous Ti coatings. So, to increase the porosity of Ti coatings beyond that obtained by depositing Ti particles alone, coatings were prepared using the CGDS process. This process enables the particles to reach higher velocities, which should modify the mechanism responsible for incorporating Cu particles into the Ti coatings.

### 3.4 Effect of Cu porogen on the porosity of Ti coatings prepared by the CGDS technique

Figure 6a shows a typical SEM cross-section micrograph of an as-deposited Ti + Cu coating prepared by the CGDS technique. The dark gray particles are Ti and the light gray particles are Cu. The SEM micrograph of as-deposited Ti + Cu CGDS coating shows it is dense with almost no porosity. CGDS coatings prepared using different Ti + Cu feeder mixtures exhibited the same morphology with almost no pores.

Figure 6c showed the variation of the Cu content in the CGDS coating with respect to the Cu content in the powder feeder mixture. Increasing the particle velocity in the CGDS process enhances the efficiency of deposition of Cu, leading to an increased Cu content in the coating. This is consistent with the fact that the Cu particles in the CDGS coatings were deformed upon impact on the substrate (see Fig. 6a). As shown in Figure 6d, the porosity of all CGDS coatings was below 8%, considerably reduced compared to SWIS coatings. Again, this is due to the higher particle velocity in the CGDS process, which causes deformation on impact with the substrate, leading to denser deposits [26, 27, 28].

The coatings were leached in 5M nitric acid to dissolve the Cu porogen. As shown in Figure 6b, the SEM image of the leached coating indicates that Cu particles have been dissolved from the surface of the coating. However, they were still present in the core of the coating. Consequently, a rough surface with high porosity was formed on the coating surface, but the porosity in the bulk of the coating was not increased. The acidic solution did not reach the Cu particles embedded in the core of the coating even for coating with the highest Cu content (35 wt.%). This is because the Cu particles are not arranged in a continuous network that would allow the acidic solution to permeate through the entire thickness of the coating.

**3.5 Effect of Al porogen on the porosity of Ti coatings prepared by the SWIS technique**

Figure 7 shows the cross-section optical microscopy images of as-deposited Ti + Al coatings prepared by the SWIS technique. The gray areas are Al and the white areas are Ti particles. Al particles are distributed homogeneously throughout the coating. According to the EDX analysis, an increase in the Al content in the powder feeder mixture led to an increase of the Al content in the coating (Figure 8a). The Al content in the SWIS coating is larger than the Al content in the feeder, in contrast to the Ti + Cu coating deposited by the SWIS technique (see Figure 5a) and the results of Ti + Ni prepared by Nikbakht *et al.* [40]. This is thought to be due to the lower density of Al compared to Cu and Ni, which causes Al particles to reach higher velocities, and perhaps also to the higher particle temperature combined with Al's lower melting point, all of which contributing to increase the deposition efficiency [36, 40].

The porosity of the as-deposited Ti + Al coatings (Fig. 8b) was around 15% and showed no clear trend with the Al content of the powder feed mixture. This level of porosity is lower than that of SWIS coatings prepared using Ti powder (see Table 3) and lower than the porosity of SWIS coatings prepared using a mixture of Ti and Cu powders (Figure 5b). This must be linked to the ability of Al particles to deform on impact with the substrate and fill the pores formed when Ti powder alone is used.

Leaching of Ti + Al SWIS coatings was performed following the procedure described in the experimental section and cross section optical microscopy analysis was performed at different steps of the leaching process. The first step of the leaching process consisted of three successive immersion of the Ti + Al SWIS coating in 6M NaOH solution held at 70-90℃ for one hour before rinsing with deionized water. As seen in Fig. 9b, in the case of coating obtained using a Ti + Al powder mixture containing 20 wt.% Al, most of the Al particles located at the top and the sides of the coating were dissolved. However, several Al particles were still present in the coating near the

interface between the substrate and the coating. In a second step, the coating was immersed in 0.5 M $H_2SO_4$ to detach it from the substrate (see the experimental section for details). Once detached from the substrate, the self-supported coating was leached three more times in NaOH to dissolve the remaining Al particles. At the end of the process, all the Al particles were dissolved without causing any damage to the self-supported coating that kept its mechanical integrity (Figure 9c). After leaching, the Al content in the self-supported coating was close to zero (Figure 8a) and the porosity increased to *ca.* 60%, as shown in Figure 8c.

The same leaching treatment was applied to Ti + Al SWIS coating obtained using a powder mixture containing 40 and 60 wt.% Al. In both cases, complete disintegration of the coatings were observed, indicating that the aluminum content of these samples is so large that the number of contacts between the Ti particles is not large enough to guaranty the mechanical integrity of the sample once the Al particles were dissolved.

## 4. Conclusion

Self-supported porous Ti electrodes with thickness exceeding 2 mm and geometrical area exceeding 1 $cm^2$ could be prepared by SWIS deposition. The final porosity of these coating was *ca.* 60%, larger than that obtained from Ti-based PTL prepared by the powder sintering process [41], cold spray [30, 31], and vacuum plasma spray process [42]. This was achieved through the use of an Al porogen that was leached out of the coating through dissolution in an alkaline solution. The optimum concentration of Al porogen in the powder feeder mixture was 20 wt.%. At this concentration, Al could be dissolved, creating an open pore network while preserving the mechanical integrity of the resulting electrode.

## Acknowledgement

We would like to acknowledge the financial support on the Natural Sciences and Engineering Research Council (NSERC) of Canada (grant number STPGP 521504-18).

## References

[1] A. Plamen, D. N. Vito and M. Stephen, "From Hydrogen Manifesto, through Green Deal and Just Transition, to Clean Energy Act," *Electrochemical Society,* vol. 30, no. 57, 2021.

[2] A. Ajanovic, M. Sayer and R. Haas, "The economics and the environmental benignity of different colors of hydrogen," *International Journal of Hydrogen Energy,* vol. 47, no. 57, 2022.

[3] S. Shiva Kumar and V. Himabindu, "Hydrogen production by PEM water electrolysis – A review," *Materials Science for Energy Technologies,* vol. 2, no. 3, pp. 442-454, 2019.

[4] P. Ayivor, J. Torres, J. Torres, R. Van Der Pluijm and B. Stouwie, "Modelling of Large Size Electrolyzer for Electrical Grid Stability Studies in Real Time Digital Simulation," *3rd International Hybrid Power Systems Workshop,* 2018.

[5] A. Mayyas, M. Ruth, B. Pivovar, G. Bender, K. Wipke, A. Mayyas, M. Ruth, B. Pivovar, G. Bender and K. Wipke, "Manufacturing Cost Analysis for Proton Exchange Membrane Water Electrolyzers," National Renewable Energy Laboratory, Golden, CO (United States), 2019.

[6] G. Schmidt, M. Suermann, B. Bensmann, R. Hanke-Rauschenbach and I. Neuweiler, "Modeling Overpotentials Related to Mass Transport Through Porous Transport Layers of PEM Water Electrolysis Cells," *Journal of The Electrochemical Society,* vol. 167, no. 11, 2020.

[7] X. Z. Yuan, N. Shaigan, C. Song, M. Aujla, V. Neburchilov, J. T. H. Kwan, D. P. Wilkinson, A. Bazylak and K. Fatih, "The porous transport layer in proton exchange membrane water electrolysis: perspectives on a complex component," *Sustainable Energy and Fuels,* vol. 6, no. 8, pp. 1824-1853, 2022.

[8] H. Becker, L. Castanheira and G. Hinds, "Local measurement of current collector potential in a polymer electrolyte membrane water electrolyser," *Journal of Power Sources,* vol. 448, 2020.

[9] S. A. Grigoriev, P. Millet, S. A. Volobuev and V. N. Fateev, "Optimization of porous current collectors for PEM water electrolysers," *International Journal of Hydrogen Energy,* vol. 34, no. 11, pp. 4968-4973, 2009.

[10] H. Ito, T. Maeda, A. Nakano, C. M. Hwang, M. Ishida, A. Kato and T. Yoshida, "Experimental study on porous current collectors of PEM electrolyzers," *International Journal of Hydrogen Energy,* vol. 37, no. 9, pp. 7418-7428, 2012.

[11] W. Ji, S. Wang, Y. Sun, H. Lv, X. Shen and C. Zhang, "Research on the influence of collector microstructure on the performance of pem electrolyzer," *World Electric Vehicle Journal,* vol. 12, no. 4, 2021.

[12] L. Zielke, A. Fallisch, N. Paust, R. Zengerle and S. Thiele, "Tomography based screening of flow field / current collector combinations for PEM water electrolysis," *RSC Advances,* vol. 4, no. 102, pp. 58888-58894, 2014.

[13] H. Ito, "Current Collectors (GDLs) and Materials," in *PEM Electrolysis for Hydrogen Production*, CRC Press, 2015.

[14] J. O. Majasan, F. Iacoviello, P. R. Shearing and D. J. Brett, "Effect of microstructure of porous transport layer on performance in polymer electrolyte membrane water electrolyser," *Energy Procedia,* vol. 151, pp. 111-119, 2018.

[15] A. S. Pushkarev, I. V. Pushkareva, M. A. Solovyev, M. Prokop, T. Bystron, S. K. Rajagopalan, K. Bouzek and S. A. Grigoriev, "On the influence of porous transport layers parameters on the performances of polymer electrolyte membrane water electrolysis cells," *Electrochimica Acta,* vol. 399, 2021.

[16] K. Zhenye, J. M.Alia, L.Young and B. Guido, "Effects of various parameters of different porous transport layers in proton exchange membrane water electrolysis," *Electrochimica Acta,* vol. 354, 2020.

[17] J. K. Lee, C. H. Lee and A. Bazylak, "Pore network modelling to enhance liquid water transport through porous transport layers for polymer electrolyte membrane electrolyzers," *Journal of Power Sources,* vol. 437, 2019.

[18] J. K. Lee, C. H. Lee, K. F. Fahy, P. J. Kim, J. M. LaManna, E. Baltic, D. L. Jacobson, D. S. Hussey, S. Stiber, A. S. Gago and K. A. A. Friedrich, "Spatially graded porous transport layers for gas evolving electrochemical energy conversion: High performance polymer electrolyte membrane electrolyzers," *Energy Conversion and Management,* vol. 226, 2020.

[19] H. Ito, T. Maeda, A. Nakano, A. Kato and T. Yoshida, "Influence of pore structural properties of current collectors on the performance of proton exchange membrane electrolyzer," *Electrochimica Acta,* vol. 100, pp. 242-248, 2013.

[20] J. Mo, Z. Kang, S. T. Retterer, D. A. Cullen, T. J. Toops, J. B. Green, M. M. Mench and F. Y. Zhang, "Discovery of true electrochemical reactions for ultrahigh catalyst mass activity in water splitting," *Science Advances,* vol. 2, no. 11, 2016.

[21] F. J. Hackemüller, E. Borgardt, O. Panchenko, M. Müller and M. Bram, "Manufacturing of Large-Scale Titanium-Based Porous Transport Layers for Polymer Electrolyte Membrane Electrolysis by Tape Casting," *Advanced Engineering Materials,* vol. 21, no. 6, pp. 1-10, 2019.

[22] H. Ito, T. Maeda, A. Nakano, C. M. Hwang, M. Ishida, A. Kato and T. Yoshida, "Experimental study on porous current collectors of PEM electrolyzers," *International Journal of Hydrogen Energy,* vol. 37, no. 9, pp. 7418-7428, 2012.

[23] G. Ryan, A. Pandit and D. P. Apatsidis, "Fabrication methods of porous metals for use in orthopaedic applications," *Biomaterials,* vol. 27, no. 13, pp. 2651-2670, 2006.

[24] M.J.Lance, J.A.Haynes and B.A.Pint, "Performance of vacuum plasma spray and HVOF bond coatings at 900° and 1100 °C," *Surface and Coatings Technology,* vol. 337, pp. 136-140, 2018.

[25] E. IRISSOU and L.-P. LEFEBVRE, "Porous metal coatings using shockwave induced spraying". Canada Patent WO/2017/191611, 05 05 2017.

[26] C. Cao, W. Li, Z. Zhang, X. Yang and Y. Xu, "Cold Spray Additive Manufacturing of Ti6Al4V: Special Nozzle Design Using Numerical Simulation and Experimental Validation," *Coatings,* vol. 12, no. 2, p. 210, 2022.

[27] H. Assadi, F. Gärtner, T. Stoltenhoff and H. Kreye, "Bonding mechanism in cold gas spraying," *Acta Materialia,* vol. 51, no. 15, pp. 4379-4394, 2003.

[28] A. Moridi, E. J. Stewart, A. Wakai, H. Assadi, F. Gartner, M. Guagliano, T. Klassen and M. Dao, "Solid-state additive manufacturing of porous Ti-6Al-4V by supersonic impact," *Applied Materials Today,* vol. 21, 2020.

[29] M. Karimi, G. W. Rankin and B. Jodoin, "Shock-wave induced spraying: Gas and particle flow and coating analysis," *Surface and Coatings Technology,* vol. 207, pp. 435-442, 2012.

[30] J. Sun, Y. Han and K. Cui, "Innovative fabrication of porous titanium coating on titanium by cold spraying and vacuum sintering," *Materials Letters,* vol. 62, no. 21-22, pp. 3623-3625, 2008.

[31] D. Qiu, M. Zhang and L. Grøndahl, "A novel composite porous coating approach for bioactive titanium-based orthopedic implants," *Journal of Biomedical Materials Research - Part A,* vol. 101 A, no. 3, pp. 862-872, 2013.

[32] F. Robitaille, M. Yandouzi, S. Hind and B. Jodoin, "Metallic coating of aerospace carbon/epoxy composites by the pulsed gas dynamic spraying process," *Surface and Coatings Technology,* vol. 203, no. 19, pp. 2954-2960, 2009.

[33] B. Jodoin, P. Richer, G. Bérubé, L. Ajdelsztajn, A. Erdi-Betchi and M. Yandouzi, "Pulsed-Gas Dynamic Spraying: Process analysis, development and selected coating examples," *Surface and Coatings Technology,* vol. 201, no. 16-17, pp. 7544-7551, 2007.

[34] M. Karimi, B. Jodoin and G. Rankin, "Shock-Wave-Induced Spraying: Modeling and Physics of a New Spray Process," *Journal of Thermal Spray Technology,* vol. 20, no. 4, pp. 866-881, 2011.

[35] M. Karimi, G. W. Rankin and B. Jodoin, "Shock-wave induced spraying: Gas and particle flow and coating analysis," *Surface and Coatings Technology,* vol. 207, pp. 435-442, 2012.

[36] H. Assadi, T. Schmidt, H. Richter, J. O. Kliemann, K. Binder, F. Gärtner, T. Klassen and H. Kreye, "On parameter selection in cold spraying," *Journal of Thermal Spray Technology,* vol. 20, no. 6, pp. 1161-1176, 2011.

[37] D. Goldbaum, R. R. Chromik, S. Yue, E. Irissou and J. G. Legoux, "Mechanical property mapping of cold sprayed Ti splats and coatings," *Journal of Thermal Spray Technology,* vol. 20, no. 3, pp. 486-496, 2011.

[38] T. Schmidt, H. Assadi, F. Gärtner, H. Richter, T. Stoltenhoff, H. Kreye and T. Klassen, "From particle acceleration to impact and bonding in cold spraying," *Journal of Thermal Spray Technology,* vol. 18, no. 5-6, pp. 794-808, 2009.

[39] E. Osarolube, I. O. Owate and N. C. Oforka, "Corrosion behaviour of mild and high carbon steels in various acidic media," *Scientific Research and Essays,* vol. 3, no. 6, pp. 224-228, 2008.

[40] R. Nikbakht, H. Assadi, K. Jahani, M. Saadati and B. Jodoin, "Cold spray deformation and deposition of blended feedstock powders not necessarily obey the rule of mixture," *Surface and Coatings Technology,* vol. 424, pp. 1-15, 2021.

[41] E. Borgardt, O. Panchenko, F. J. Hackemüller, J. Giffin, M. Bram, M. Müller, W. Lehnert and D. Stolten, "Mechanical characterization and durability of sintered porous transport layers for polymer electrolyte membrane electrolysis," *Journal of Power Sources,* vol. 374, pp. 84-91, 2018.

[42] C. Jaeggi, R. Mooser, V. Frauchiger and P. Wyss, "3D characterization of open porous vacuum plasma sprayed titanium coatings by means of high resolution micro computer tomography," *Materials Letters,* vol. 63, no. 30, pp. 2643-2645, 2009.

[43] M. A. Khan, H. Zhao, W. Zou, Z. Chen, W. Cao, J. Fang, J. Xu, L. Zhang and J. Zhang, "Recent Progresses in Electrocatalysts for Water Electrolysis," *Electrochemical Energy Reviews,* vol. 1, no. 4, pp. 483-530, 2018.

[44] C. Santoro, A. Lavacchi, P. Mustarelli, V. Di Noto, L. Elbaz, D. R. Dekel and F. Jaouen, "What is Next in Anion-Exchange Membrane Water Electrolyzers? Bottlenecks, Benefits, and Future," *ChemSusChem,* vol. 15, no. 8, 2022.

[45] S. M. Steen, J. Mo, Z. Kang, G. Yang and F. Y. Zhang, "Investigation of titanium liquid/gas diffusion layers in proton exchange membrane electrolyzer cells," *International Journal of Green Energy,* vol. 14, no. 2, pp. 162-170, 2017.

[46] R. Maric and H. Yu, "Proton Exchange Membrane Water Electrolysis as a Promising Technology for Hydrogen Production and Energy Storage," *Intech,* 2018.

[47] A. Pozio, F. Bozza, G. Nigliaccio, M. Platter and G. Monteleone, "Development perspectives on low-temperature electrolysis," *Energia, ambiente e innovazione,* pp. 66-71, 2021.

[48] C. V. Pham, D. K. Escalera-López, S. Cherevko and S. Thiele, "Essentials of High Performance Water Electrolyzers – From Catalyst Layer Materials to Electrode Engineering," *Advanced Energy Materials,* vol. 11, no. 44, 2021.

[49] M. Bernt, A. Hartig-Weiß, M. F. Tovini, H. A. El-Sayed, C. Schramm, J. Schröter, C. Gebauer and H. A. Gasteiger, "Current Challenges in Catalyst Development for PEM Water Electrolyzers," *Chemie-Ingenieur-Technik,* vol. 92, no. 1-2, pp. 31-39, 2020.

[50] O. F. Selamet and M. S. Ergoktas, "Effects of bolt torque and contact resistance on the performance of the polymer electrolyte membrane electrolyzers," *Journal of Power Sources,* vol. 281, pp. 103-113, 2015.

[51] C. C. Weber, T. Schuler, R. De Bruycker, L. Gubler, F. N. Büchi and S. De Angelis, "On the role of porous transport layer thickness in polymer electrolyte water electrolysis," *Journal of Power Sources Advances,* vol. 15, 2022.

[52] J. Parra-Restrepo, R. Bligny, J. Dillet, S. Didierjean, D. Stemmelen, C. Moyne, A. Degiovanni and G. Maranzana, "Influence of the porous transport layer properties on the mass and charge transfer in a segmented PEM electrolyzer," *International Journal of Hydrogen Energy,* vol. 45, no. 15, pp. 8094-8106, 2020.

[53] H. G. Merkus, Particle Size Measurements: Fundamentals, Practice, Quality, Springer Science & Business Media, 2009.

[54] F. Saba, E. Garmroudi-Nezhad, F. Zhang and L. Wang, "Fabrication, mechanical property and in vitro bioactivity of hierarchical macro-/micro-/nano-porous titanium and titanium molybdenum alloys," *Journal of Materials Research,* vol. 35, no. 19, pp. 2597-2609, 2020.

[55] F. Contu, B. Elsener and H. Böhni, "Serum effect on the electrochemical behaviour of titanium, Ti6Al4V and Ti6Al7Nb alloys in sulphuric acid and sodium hydroxide," *Corrosion Science,* vol. 46, no. 9, pp. 2241-2254, 2004.

[56] J. Lee, W. Gao, Z. Li and Y. He, "Corrosion behaviour of Ti3Al and Ti3Al–11 at.% Nb intermetallics," *Materials Letters,* vol. 57, no. 9-10, pp. 1528-1538, 2003.

[57] L. Wang, Y. Xu, S. Yu, T. Bai, W. Zhou, Z. Yu and L. Zhou, "Improvement on biosafety and bioactivity of Ti–6Al–4V alloys by construction the three-dimensional grid structure though electrochemical dealloying," *Journal of Materials Research and Technology,* vol. 17, pp. 546-559, 2022.

[58] A. Mogoda, Y. Ahmad and W. Badawy, "Corrosion behaviour of Ti-6Al-4V alloy in concentrated hydrochloric and sulphuric acids," *Journal of Applied Electrochemistry,* vol. 34, no. 9, pp. 873-878, 2004.

Figure

Click here to access/download;Figure;Papier_Ti_Skeleton_NRC_version6.pptx

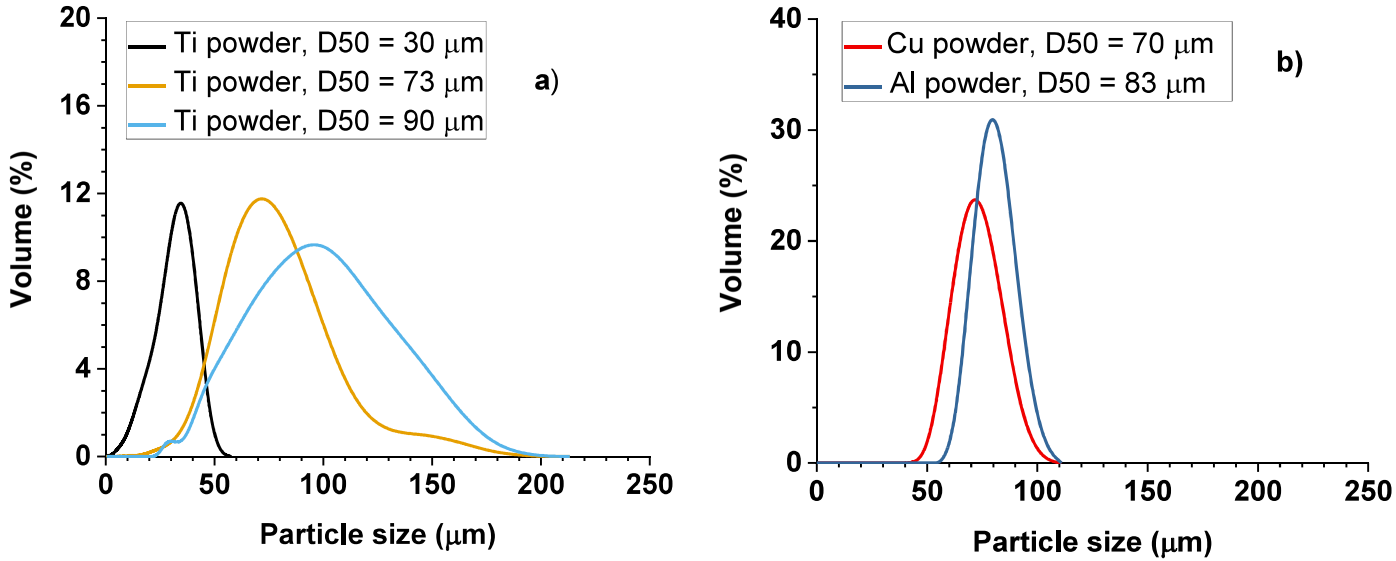


Figure 1: Particle size distribution of the powders used in the present study: a) Ti powders and b) Al and Cu powders.

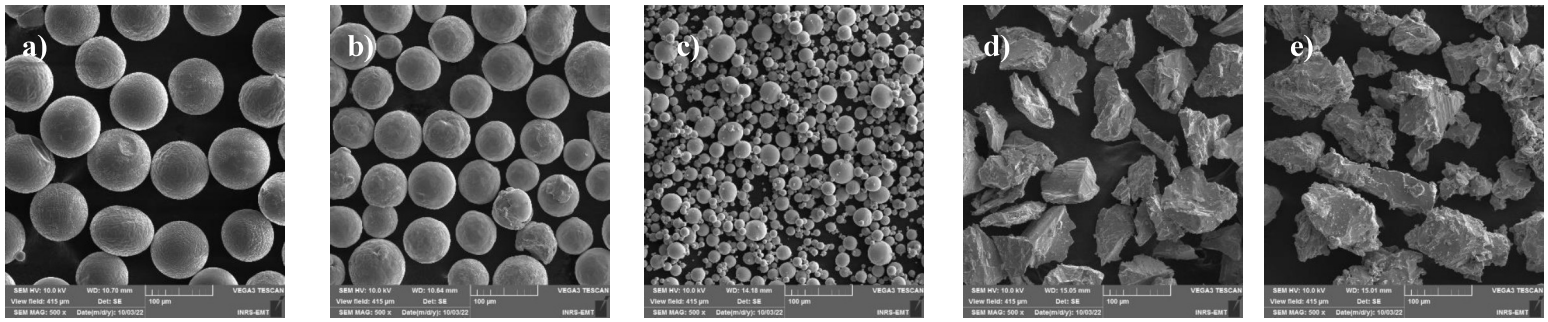


Figure 2: SEM micrographs of three different Ti powders and two different porogens used for the preparation of the CS and SWIS coatings. a) Al, b) Cu, c) Ti (D50 = 30 μm), d) Ti (D50 = 73 μm) and e) Ti (D50 = 90 μm).

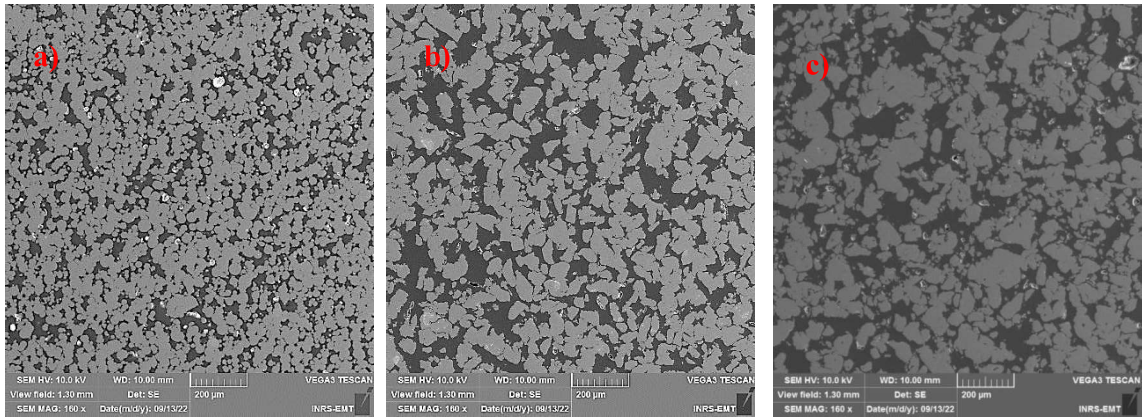


Figure 3: SEM cross-section of SWIS coatings prepared using Ti particles of different sizes a) D50 = 30 µm, b) D50 = 73 µm, and c) D50 = 90 µm samples.

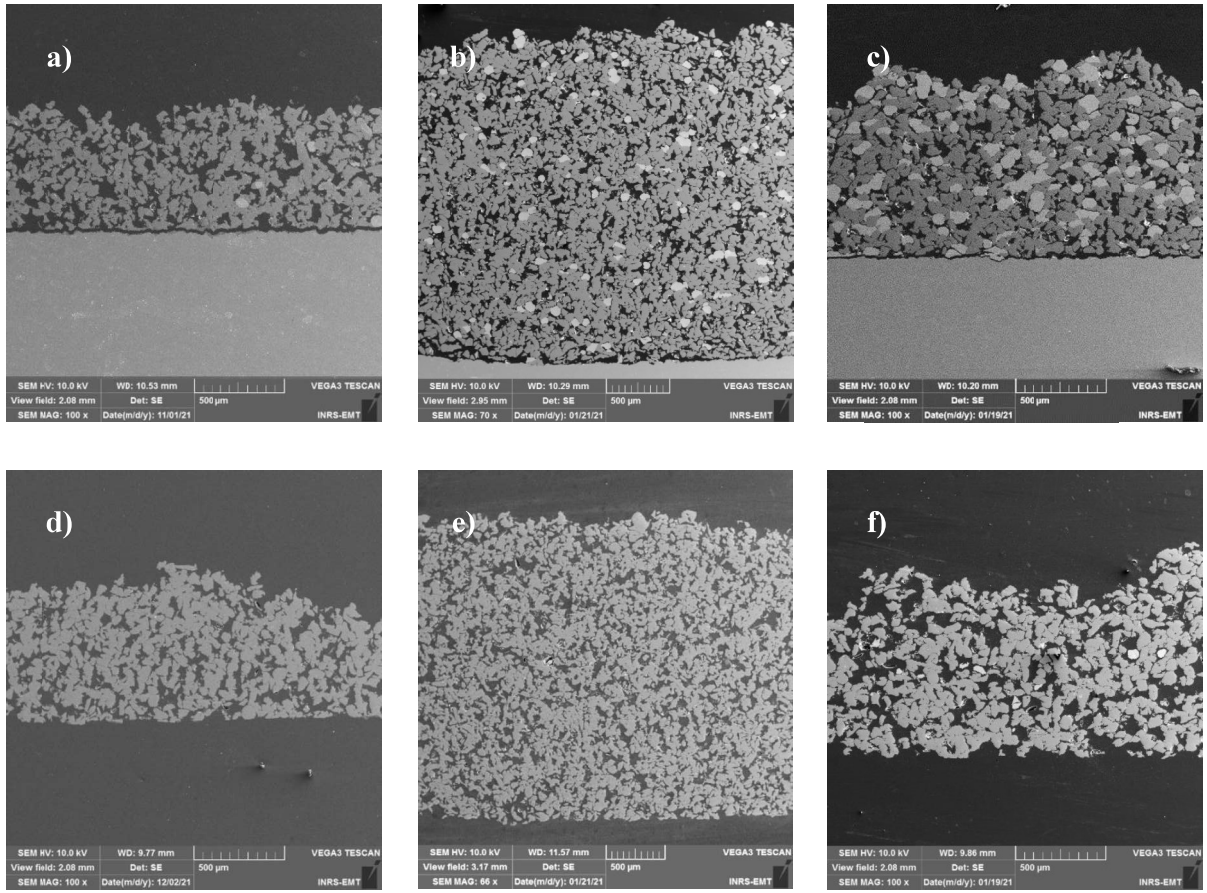


Figure 4: SEM cross-section of Ti + Cu coatings prepared by the SWIS technique. The Ti + Cu powder feeder composition was a) 5 wt.%, b) 30 wt.% and c) 60 wt.%. The as-deposited samples are shown in a), b) and c) respectively. Samples after leaching in $HNO_3$ are shown in d), e) and f).

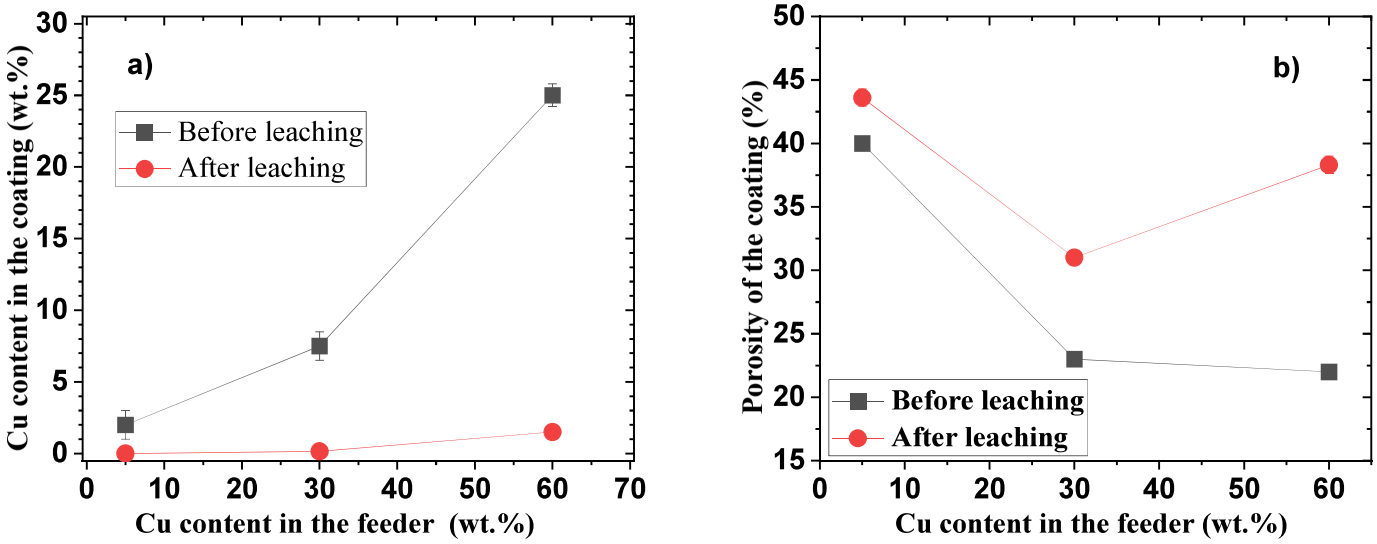


Figure 5: Variation of a) the Cu content and b) porosity of coatings prepared by the SWIS technique with respect to the Cu content in the powder feeder mixture.

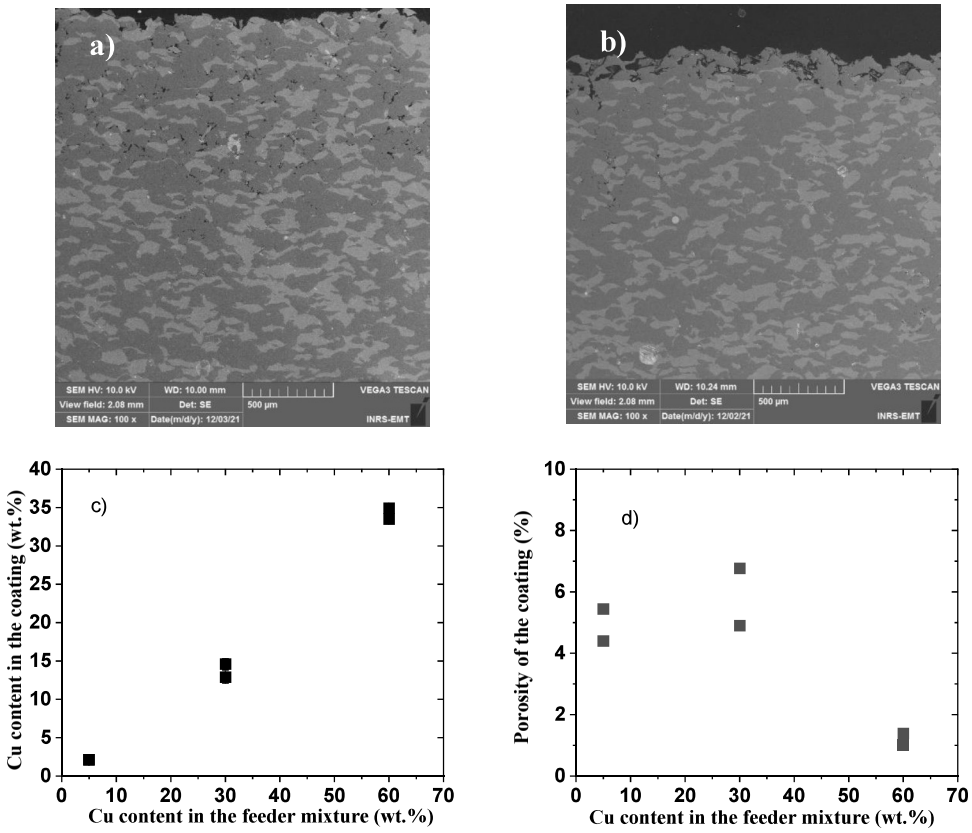


Figure 6: Cross-section SEM micrographs of Ti + Cu CGDS coatings prepared from mixture containing 60 wt.% of Al. In a), as-deposited and b) after leaching. The variation of the Cu content in the as-deposited coating with respect to the Cu content in the feeder mixture is given in c), with the corresponding variation of the coating porosity in d).

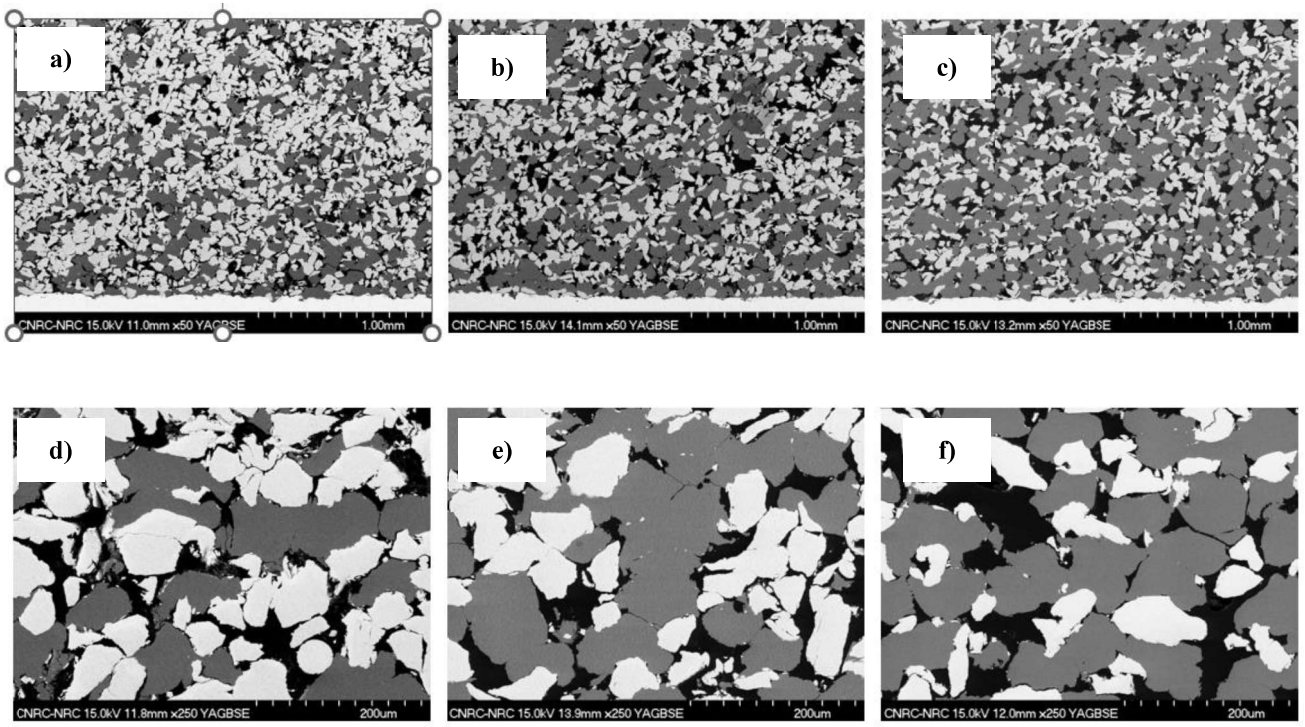


Figure 7: Cross-Section Optical Microscopy of Ti + Al coatings prepared from powder mixture containing a) and d) 20wt.% Al, b) and e) 30 wt.% Al, and c) and f) 40 wt.% Al. The grey areas correspond to Al particles, while the white areas were Ti particles.

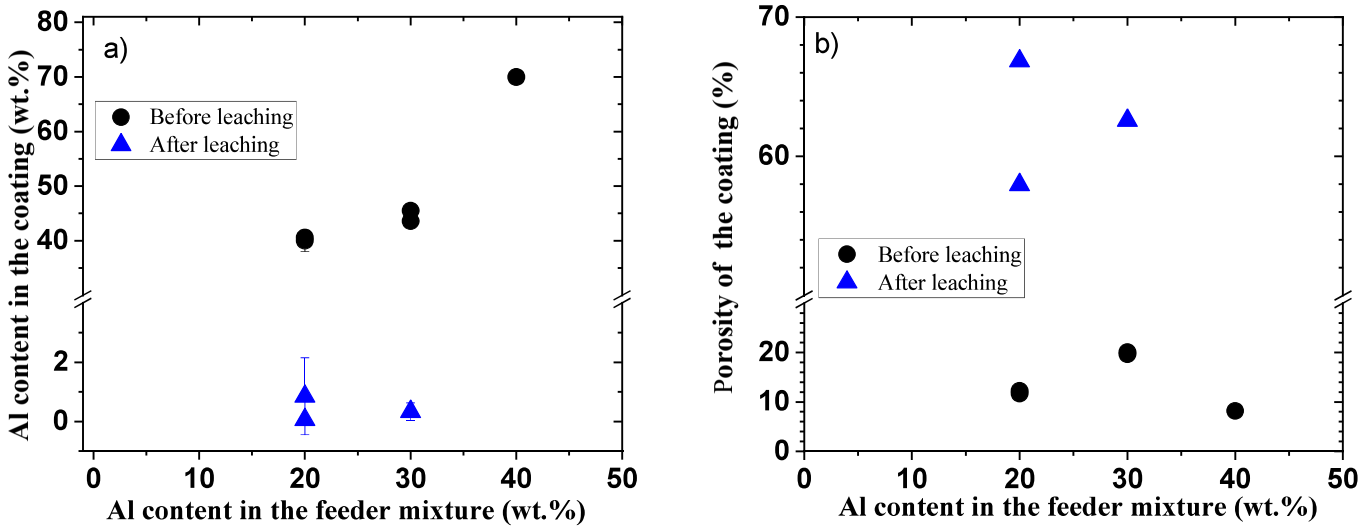


Figure 8: In a), variation of Al content of the coating with respect to the Al content of the feeder mixture. In b) variation of the porosity of the coating with respect to the Al content of the feeder mixture.

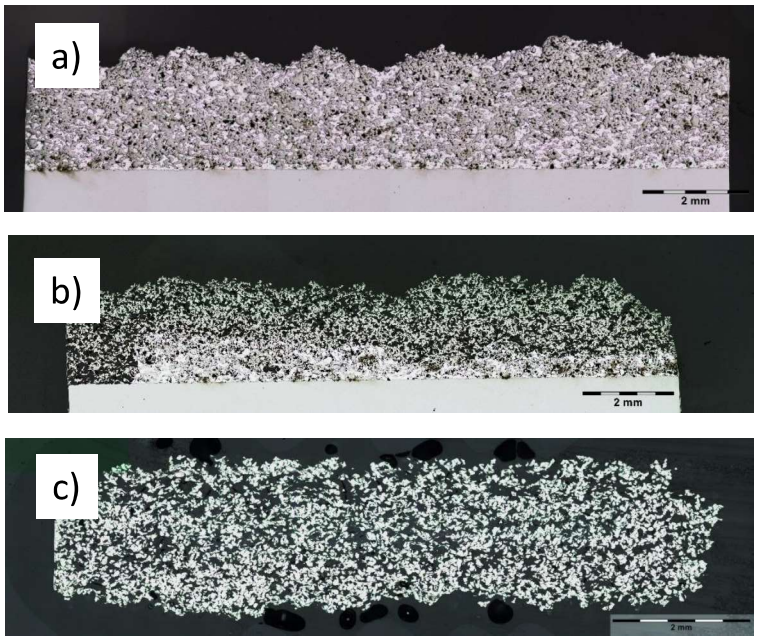


Figure 9: Cross-section optical microscopy of Ti + Al coating prepared from a powder mixture containing 20 wt.% Al: a) as-deposited, b) after three leaching cycles, and c) after a subsequent leaching in NaOH once the coating was detached from the substrate. The details of the leaching procedure are given in the experimental section.

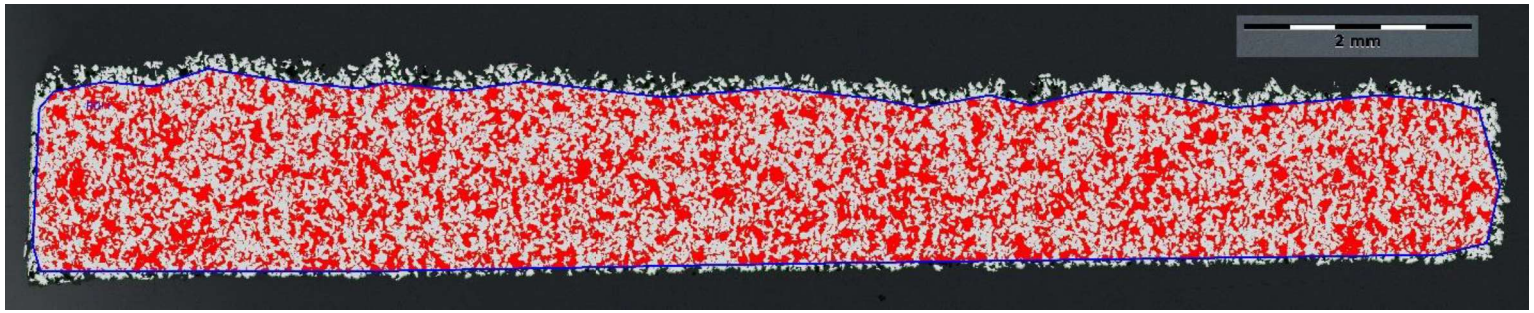


Figure S1: Typical example of a cross-section optical microscopy image used to estimate the porosity of coatings. The sample shown was a Ti coating prepared by the SWIS technique using Ti powder with D50 = 73 μm. The white areas are the Ti particles, while the red area are the pores.

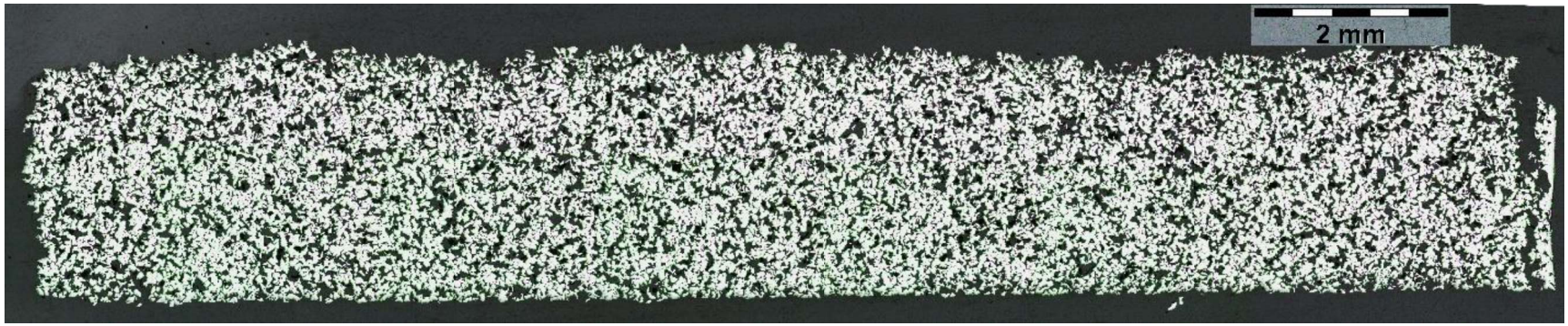


Figure S2: Ti + Cu with 30 wt.% Cu after leaching in $HNO_3$. All Cu particles are dissolved from the coating. Also, the coating is detached from the substrate.